frontiers | Frontiers in Earth Science

TYPE Original Research
PUBLISHED 19 January 2023
DOI 10.3389/feart.2023.1104831

OPEN ACCESS

EDITED BY
Zilong Zhou,
Central South University, China

REVIEWED BY
Fengqiang Gong,
Southeast University, China
Yunliang Tan,
Shandong University of Science and Technology, China

*CORRESPONDENCE
Taotao Du,
yl_dutt@126.com

SPECIALTY SECTION
This article was submitted to Geohazards and Georisks, a section of the journal Frontiers in Earth Science

RECEIVED 22 November 2022
ACCEPTED 03 January 2023
PUBLISHED 19 January 2023

CITATION
Du T, Pan J, Xia Y and Sun R (2023), Study on the influence of confining pressure and unloading damage on the bursting liability characteristics of coal.
Front. Earth Sci. 11:1104831.
doi: 10.3389/feart.2023.1104831

Study on the influence of confining pressure and unloading damage on the bursting liability characteristics of coal

Taotao Du[1,2,3]*, Junfeng Pan[1,2,3], Yongxue Xia[1,2,3] and Ruda Sun[1,2,3]

[1]CCTEG Coal Mining Research Institute, Beijing, China, [2]China Coal Research Institute, Beijing, China, [3]Coal Mining and Designing Department, Tiandi Science and Technology Co., Ltd., Beijing, China

The research on the bursting liability of coal under confining pressure and unloading damage is critical in creating prevention mechanisms for coal mass rock bursts in deep underground mines. Cyclic loading and unloading tests of variable stress with a lower limit were performed under multistage confining pressure and different amplitude unloading to explore their influence on the impact tendency of the coal bodies. Meanwhile, the characteristic parameter analysis of acoustic emissions was used to evaluate the failure. The results revealed that the accumulated number and energy of acoustic emission events gradually decreased with increasing the confining pressure. The coal specimen became denser, and the failure mode gradually transitioned from brittle to ductile. With the increase in unloading amplitude, the cumulative number of acoustic emission events in the coal specimens decreases, the damage degree to the coal body increases, the peak load decreases, and the failure mode transitions from ductile to brittle. The increase in confining pressure results in an increase in the input energy and the elastic strain energy, while the increase in the unloading range of the coal body leads to a decrease in the input energy and elastic strain energy. In addition, after the confining pressures of 3 MPa, 6 MPa, and 9 MPa, the residual elastic energy index of the coal specimens increases by 21.76%, 42.92%, and 71.69%, respectively, compared with the room pressure conditions. The residual elastic energy index decreases by 21.11% and 55.38% for the unloading amplitude of 3 MPa and 6 MPa, respectively, compared with the unloaded coal specimen, indicating that the impact tendency of the coal body is enhanced by the confining pressure conditions.

KEYWORDS

coal, bursting liability, confining pressure, unloading effect, residual elastic energy index

1 Introduction

Global demand for coal has increased unabated (Wang et al., 2022). The technical equipment and organization mode of coal mining are constantly improved; In recent years, technologies such as intelligent, high-yield, and efficient working faces in large and medium-sized mines and rapid excavation of self-formed roadways have developed for effective mining practices (Wang and Huang, 2017; Zhang et al., 2020). The continuous progress of coal mining technology has accelerated the development of shallow coal resources and gradually shifted to deeper resources. Compared with shallow sections, the deep underground environment has higher *in-situ* stress, higher geothermal temperature, higher osmotic pressure, and strong mining disturbances not typically encountered in the shallower resources (Xie et al., 2021). Coal bursts are one of the most serious forms of dynamic hazard of the surrounding rock caused by

deep coal mining. Most coal bursts occur in the vicinity of stopes or roadways (Cai et al., 2016), which is referred to as the impact liability of coal. It is the phenomenon that the energy stored in the coal is released and produces impact damage under the combined action of several external physical fields (Gong et al., 2019). The greater the bursting liability of coal, the greater the failure intensity and influence range of rock burst. The study of the mechanism of coal bursting is crucial to the determination of liability, early warning, and prevention of accidents.

The above bursting liability indexes are generally determined only by uniaxial compression tests at room temperature and pressure. However, coal bodies exhibit different mechanical properties in deep geological environments because of the high stress and mining influence. Ding et al. (2022) studied the effects of two cyclic loading and unloading modes on the mechanical damage characteristics of coal in a triaxial confining pressure environment. Li et al. (2022a) investigated the effect of strain rate and confining pressure on the mechanical failure behavior of coal. Xie et al. (2012) analyzed the effects of different mining layouts on the mechanical properties of coal. Li et al. (2022b) conducted an experimental study on the influence of confining pressure and bedding angle on the mechanical properties of coal. Yang et al. (2021a) conducted an experimental study on the fracture behavior of coal under different confining pressures. Zhou H. W. et al. (2022) researched the evolution of fracture and pore structure of coal under confining and axial compressive loads. The roof of cutting and pressure relief technology effectively controls rock burst disasters induced by underground coal mining (Wang Q. et al., 2020). This technology generally uses hydraulic fracturing (Yang et al., 2018a; Yang et al., 2020a; Yang et al., 2021b), directional blasting, and other methods to pre-fracture the overlying roof and unload the surrounding rock pressure, achieving the purpose of reducing the influence of rockburst hazards to a certain extent. The unloading effect damages the coal body and affects the mechanical properties of the coal body, which in turn affects the impact characteristics. Liu Q. et al. (2017) performed mechanical tests on coal under two different stress unloading paths and discussed the influence of confining pressure unloading on soft coal strength to provide a basis for borehole stability analysis. Yin et al. (Yin et al., 2013; Yin et al., 2015) researched coal geomechanical and flow properties under axial loading stress and unloading confining pressure tests. Zhang et al. (2017) conducted an experimental study on the mechanical behavior of reconstructed coal samples under different unloading confining pressures. Wang D. et al. (2020) studied the seepage characteristics of coal under unloading confining pressure. Zhou et al. (2019) analyzed the creep law of deep coal under the action of releasing confining pressure. Kong et al. (Kong et al., 2020) studied the dynamic mechanical characteristics and fracture mechanism of gas and coal after unloading damage. However, there are few reports on the influence of confining pressure and unloading conditions on coal bursting liability.

Various indicators have been proposed to evaluate the bursting liability of coal, including uniaxial compressive strength (σ_c) (Zhou J. et al., 2022), impact energy index (K_E) (Liu X. et al., 2017), elastic energy index (W_{ET}) (Kidybinski, 1981), dynamic failure time (D_T) (Ouyang et al., 2015), impact energy velocity index (W_{ST}) (Guo et al., 2018), modulus index (K_λ) (Yang X. et al., 2018) and residual elastic energy index (C_{EF}) (Gong et al., 2020), *etc.* Gong et al. (2022) compared more than ten indexes to determine the bursting liability of coal and concluded that C_{EF} was the most accurate for predicting the bursting liability of various coal bodies.

To this end, the cyclic loading and unloading tests with variable stress limits under different confining pressure conditions and under different amplitudes of unloading conditions were carried out in this paper. In addition, an acoustic emission system was used for real-time monitoring. The bursting liability of coal samples under different conditions was compared and analyzed to investigate the impact properties of deep-seated coal.

2 Experiment overview

2.1 Sample preparation

The non-stick coal samples collected from a coal mine in the southern Ordos Basin in Inner Mongolia at a depth of about 425 m were studied in this paper. According to industrial analysis, the samples have a vitrinite reflectance of 0.87%, ash content of 8.89%, average moisture content of 0.83%, and volatile matter of 30.37%. The coal samples were obtained *in situ* to avoid damage to the original coal samples caused by external factors. Wax sealing was carried out to reduce the influence of weathering *in situ*. To reduce the impact of mechanical damage on subsequent tests, a wire-cutting with a numerically-controlled machine tool was used to process the specimens (Yang et al., 2019a; Yang et al., 2020b). According to the International Society of Rock Mechanics standard, each coal sample was made into a cylindrical specimen with a diameter of 50 mm and a height of 100 mm. The dimensional error of the processed specimen needed to be less than 2 mm and the unevenness of the upper and lower end faces of the specimen after cutting were less than ±0.05 mm. The end face was perpendicular to the axis of the specimen, and the maximum deviation was less than 0.25°. To minimize the influence of sample inhomogeneity, all specimens were taken from the same coal body in the same coring direction. Specimens with similar densities and wave speeds were selected for subsequent experimental research.

2.2 Test equipment

In this study, the SAS-2000 coal and rock static disturbance triaxial pressure test system was used (as shown in Figure 1). The test system consists of a loading and unloading module, a confining pressure environment simulation module, a deformation monitoring module, an acoustic emission (AE) monitoring module, a control module, and a data acquisition module. The maximum axial pressure applied to the coal rock mass sample is 380 MPa, and the maximum confining pressure is 160 MPa. The control accuracy of the internal pressure sensor is 0.005 MPa with a resolution of 5×10^{-4} MPa. The loading methods include displacement control and load control, and the adjustable ranges of the two loading methods are 0.0001~1 mm s^{-1} and 0.005~1 kN s^{-1}. In addition, the accuracy of the axial and radial deformation measurement device of the coal rock specimen is 0.0005 mm, and the resolution is 5×10^{-5} mm. Both axial and radial effective deformations were measured within ±8 mm. As shown in Figure 1, the experimental system is also equipped with a PCI-2 acoustic emission monitoring system (Chen et al., 2017; Chen et al., 2019), The main amplifier of the AE test system was set to 35 dB, and

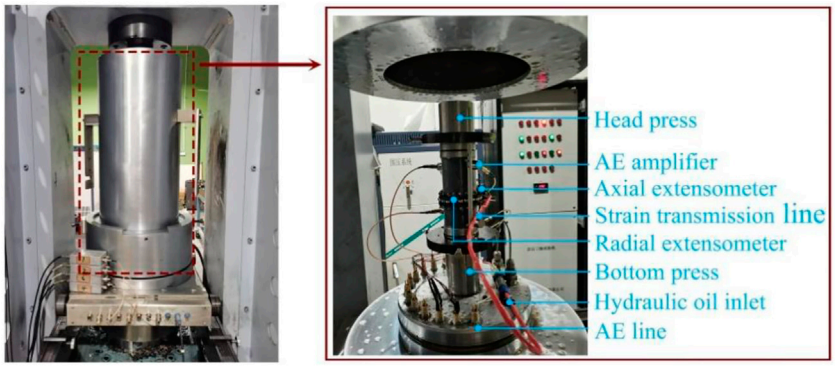

FIGURE 1
Rock mechanics test system and acoustic emission monitoring system.

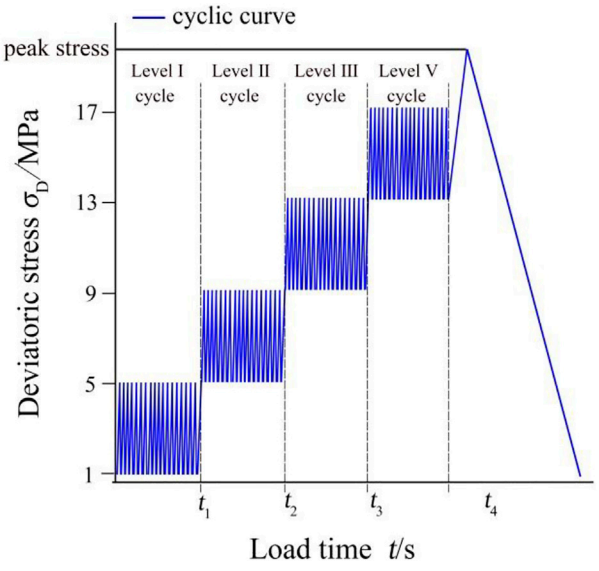

FIGURE 2
Variable stress lower limit cyclic loading and unloading mode.

the threshold was 40 dB. The sampling length of single waveform and sampling rate are set to 31.5 k and 4.5 MSPS, respectively. In order to ensure the accuracy of positioning, each coal specimen was tested with four AE sensors, allowing for real-time monitoring of the failure process of coal specimens in different confining pressure environments.

2.3 Experimental procedure

Two loading types were performed in this section. One was the lower limit cyclic loading and unloading test of coal specimens under the condition of multistage confining pressure. The other was the cyclic loading and unloading test with variable stress lower limit after different amplitude unloading confining pressure damage.

The steps of the first type of test are as follows: first, the conventional compression tests of the coal specimens were performed at different confining pressures. The confining pressure was set as the standard pressure, followed by 3 MPa, 6 MPa, and 9 MPa, respectively. The displacement control mode was used to carry out the compression test, and the loading rate was set as 0.002 mm s^{-1}. Two sets of tests were performed on the coal samples under each condition. It was obtained that the compressive strength of the coal body under multistage confining pressure and approximate static load conditions.

Next, a variable stress lower limit cyclic loading and unloading test under multistage confining pressure was carried out by using the loading control mode. The loading rate was set to 0.04 KN s^{-1}, about 0.02 MPa s^{-1}. The lower limit cyclic loading mode of variable stress is shown in Figure 2. The initial confining pressure environment was set to the standard pressure, 3 MPa, 6 MPa, and 9 MPa, respectively. The difference between the axial and confining pressures of the first-stage cyclic loading and unloading under the four confining pressure conditions was the lower limit of the deviatoric stress, set to 1 MPa. The cyclic loading and unloading amplitude was set to 4 MPa, and 30 loading and unloading operations were carried out for each cycle until the coal specimen was damaged. The preamplifier (acoustic emission probe) of the PCI-2 acoustic emission system was arranged at a predetermined position of the coal specimen to perform real-time monitoring of the damage process. Two groups of cyclic loading and unloading tests were carried out for each of the above conditions.

The steps of the second type of test are as follows: First, the confining pressure of the coal specimen was increased to 9 MPa, the axial stress was loaded to 15 MPa, and the axial pressure was always kept unchanged. The confining pressure on the coal specimen was unloaded to 6 MPa, 3 MPa, and standard pressure with an unloading rate of 0.01 MPa s^{-1} to simulate the damage process of the coal body under different unloading amplitudes. After the internal environment of the triaxial autoclave was stabilized for 1 h, the confining pressure was increased to the initial setting of 9 MPa, and then the compressive strength test was carried out. Two groups of tests were carried out under the above conditions. Finally, the load control mode was used to carry out the above-mentioned variable stress lower limit cyclic loading and unloading tests on the coal samples after unloading with different amplitudes. The specific test steps were the same as

TABLE 1 Compression test results of coal specimens under different confining pressures.

Confining pressure	Specimen number	Compressive strength σc/MPa	Average σc/MPa	Elasticity modulus E/GPa	Average elasticity modulus E/GPa
normal pressures	C-0-1	12.01	11.44	1.12	1.02
	C-0-2	10.87		.92	
3 MPa	C-3-1	17.68	16.52	1.64	1.51
	C-3-2	15.36		1.38	
6 MPa	C-6-1	23.24	21.85	2.21	2.06
	C-6-2	20.46		1.91	
9 MPa	C-9-1	28.19	26.74	2.51	2.42
	C-9-2	25.29		2.33	

TABLE 2 Compression test results of coal specimen under different amplitude unloading conditions.

Unloading value	Specimen number	Compressive strength σc/MPa	Average σc/MPa	Elasticity modulus E/GPa	Average elasticity modulus E/GPa	Deterioration degree D/%
0	C-9-1	28.19	26.74	2.51	2.42	—
	C-9-2	25.29		2.33		
−3 MPa	C-3-1	24.12	22.82	2.21	1.96	−14.7
	C-3-2	21.52		1.71		
−6 MPa	C-6-1	15.85	14.68	1.32	1.24	−45.1
	C-6-2	13.51		1.16		

those of the lower limit cyclic loading and unloading tests. Similarly, the PCI-2 acoustic emission system was used to conduct real-time monitoring of damage and fracture. Two groups of coal specimen cyclic loading and unloading tests were conducted for each condition.

2.4 Test results

The conventional compression test results of coal specimens under different confining pressure conditions are listed in Table 1. The average compressive strength of the coal samples in the atmospheric laboratory environment was 11.44 MPa, and the average elastic modulus was 1.02 GPa. When the confining pressure increased to 3 MPa, 6 MPa, and 9 MPa, the average compressive strengths of the coal specimens were 16.52 MPa, 21.85 MPa, and 26.74 MPa, respectively. Compared with the standard pressure conditions, the uniaxial compressive strength of the coal body increased by 44.5%, 91.0%, and 133.7%, respectively. The average elastic modulus increased to 1.51 GPa, 2.06 GPa, and 2.42 GPa, with improvements of 48.0%, 101.9%, and 137.3%, respectively.

The compressive strengths after increasing the confining pressure to 9 MPa and experiencing different amplitudes of unloading are listed in Table 2. At 9 MPa, the average compressive strength was 22.82 MPa, approximately 14.7% less than that before unloading. The elastic modulus decreased to 1.96 Gpa. After the confining pressure was unloaded to 3 MPa (the unloading amplitude was 6 MPa), the average compressive strength became 14.68 MPa when the confining pressure was increased to 9 MPa again. The average compressive strength underwent the unloading was 45.1% less than that without unloading. The elastic modulus decreased to 1.24 Gpa. The coal specimen was damaged when the confining pressure was unloaded to 1.56 MPa.

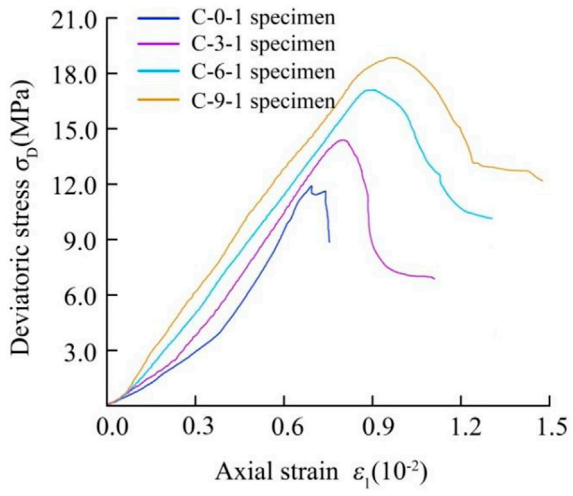

FIGURE 3
Deviatoric stress - axial strain (σ_D-ε_1) curves of coal specimen under different confining pressure.

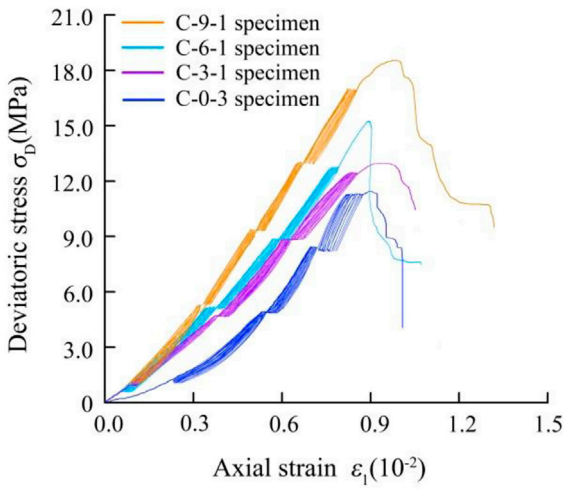

FIGURE 4
The σ_D-ε_1 curves of coal specimens with cyclic loading and unloading at different stress lower limits under the different confining pressure.

3 Experiment result and analysis

3.1 σ_D-ε_1 curves

3.1.1 σ_D-ε_1 curves of coal specimens under different confining pressure

Figure 3 shows the deviatoric stress σ_D and axial strain ε_1 curves of the entire loading compression test when the confining pressures are normal pressure, 3 MPa, 6 MPa, and 9 MPa, respectively. As the confining pressure increased, the compressive strength of coal specimens significantly improved. When the sample was subjected to initial stress, the four σ_D-ε_1 curves in the figure have a concave form. In this process, the increment of the axial strain decreased with increasing the deviatoric stress because the micro-fractures in the coal body closed under the axial load, corresponding to the compaction stage of the coal specimen (Yang et al., 2018b; Yang et al., 2019b). At the same time, with the increase in the confining pressure, the scope of this compaction stage continued to shrink, indicating that the primary micro-fractures in the coal body closed in the early stage due to the initial confining pressure. As the axial load was further applied to the coal specimen, the deviatoric stress changed linearly with the axial strain, indicating that the coal specimen underwent elastic deformation at this stage. When the axial load increased to a certain stage, the deviatoric stress decreased with the increase in the axial strain. The coal specimen entered the plastic stage after yielding and then reached the peak stress during this circle. The coal specimen was damaged. Due to the effect of confining pressure, the coal specimen entered the post-peak stress softening stage after failure. The variation trend of the deviatoric stress-lateral strain curve of the coal specimen is consistent with that of the deviatoric stress-axial strain curve.

Figure 4 shows the σ_D-ε_1 curves of variable stress lower limit cyclic loading and unloading corresponding to four confining pressure environments. The overall changing trends of the deviatoric stress-strain curve obtained under triaxial variable stress lower limit cyclic loading and unloading is consistent with those obtained by the conventional triaxial compression test under the same confining pressure. In the first stage of cyclic loading and unloading (lower stress levels), the original pores and cracks in the coal samples are gradually compacted due to repeated increases and decreases in deviatoric stresses. The four deviatoric stress-strain curves were all concave in the first stage of cyclic loading and unloading. As the number of cycles increased, the first-stage hysteresis curve's area gradually decreased. After the first stage of cyclic loading and unloading was complete, with the increase in the lower limit of the stress level, the coal specimen under multistage confining pressure entered the elastic stage. In this stage, the slopes of the deviatoric stress-strain cyclic loading and unloading curves became similar after a certain point. The area of the hysteresis curve did not change much as the number of cycles increased, especially for the coal specimen under the confining pressure environment of 9 Mpa. The second-stage cyclic loading and unloading curve had almost no apparent hysteresis phenomenon. However, compared with its compressive strength for coal sample C-0-3 under atmospheric pressure, the stress level of cyclic loading and unloading in the second stage was higher, which led to new damage inside the coal body and the connection of primary micro-cracks. This indicates that at this stage, the hysteresis curve becomes more evident with the increase in cycles. The cyclic loading and unloading series replaced by the approximate elastic variation range of the σ_D-ε_1 curve of the coal specimen under the above-confining pressure conditions were different. The number of cyclic loading and unloading stages was 1, 2, 2, and 3, respectively, which shows that with the increase in initial confining pressure, the coal specimen becomes denser, and the range of elastic stages expands continuously.

During the last stage of cyclic loading and unloading during the above test under different confining pressure conditions, the strain in the sample increased slowly with an increase in the deviatoric stress, and the area of the hysteresis loop increased significantly. In this case, the sample gradually transitioned to the plastic stage, during which the incremental strain increased significantly. Irreversible deformation continued to develop. Under normal pressure conditions, only 14 complete cycles occurred during the last cyclic loading and unloading phase before the coal specimen failed, with an increase in an axial strain of 0.75%. Under the confining pressure of 3 MPa, the last stress level before the failure of the coal specimen C-3-3 underwent one complete cycle (30 times), and the axial strain increased by 0.61%. Coal specimen C-6-3 also completed a complete loading and unloading cycle before failure in the 6 MPa confining pressure environment, and the axial strain increased by 0.42% at this stage. Under the confining pressure of 9 MPa, the axial strain of the coal specimen C-9-3 increased by 0.28% after undergoing the last complete loading and unloading cycle before failure. Overall, the increment of strain after unloading decreased. The compressive strength of the coal specimen without confining pressure after loading and unloading at the lower limit of variable stress was reduced by about 5.6% compared with the original specimen. This indicates that the coal body was damaged to a certain extent after the above cyclic loading and unloading. The compressive strength increases by about 3.1%, 4.7%, and 6.2%, respectively, after cyclic loading and unloading at the lower limit of variable stress under the confining pressure environment of 3 MPa, 6 MPa, and 9 MPa, respectively.

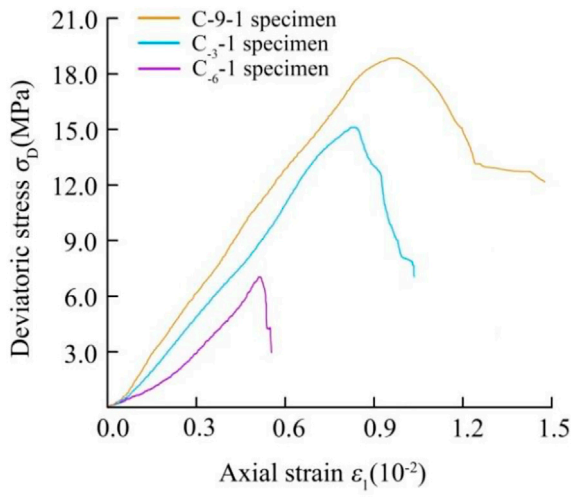

FIGURE 5
The σ_D-ε_1 curves of coal specimens under the different unloading conditions.

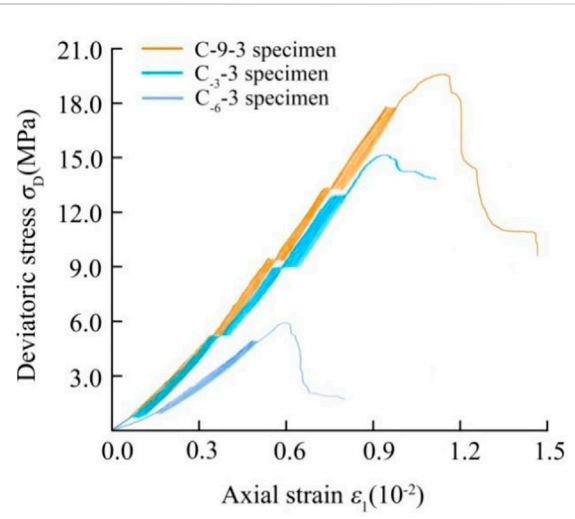

FIGURE 6
The σ_D-ε_1 curves of coal specimens with cyclic loading and unloading at different stress lower limits under different unloading conditions.

3.1.2 The σ_D-ε_1 curves of coal specimens under unloading condition

Figure 5 depicts the curves of partial stress σ_D and axial strain ε1 during the whole process of the compressive test when unloaded, unloaded to 6 MPa, and unloaded to 3 MPa in the 9 MPa perimeter pressure environment. As shown in Figure 5, with the increase of the unloading magnitude, the compressive strength of coal specimens significantly decreased when the confining pressure increased to 9 MPa again. The three types of σ_D-ε_1 curves in the figure show a depressed shape at the early stage of axial loading, which corresponds to the compaction stage of coal specimens. Furthermore, with the increase in the unloading amplitude of coal specimens, the range of this compaction stage expanded, which indicates that the unloading effect increases the micro defects in coal specimens. With the further application of the axial load on the coal specimen, the bias stress varied linearly with the axial strain, which indicates that the coal specimen undergoes the elastic deformation at this stage. When the axial load increased to a particular stage, the partial stress decreased with the increase of axial strain, during which the coal specimen yielded and then entered the plastic stage. With the increase in unloading magnitude, the peak load and the strain value corresponding to the peak stress decreased continuously. In addition, the increase in unloading degree caused the post-peak deformation decrease, and the damage gradually transitioned from ductile to brittle. The trend of the deflected stress-radial strain curve of the coal specimen was consistent with that of the deflected stress-axial strain curve.

Figure 6 shows the curves of σ_D-ε_1 for cyclic loading and unloading at the lower limit of variable stress under the above three unloading conditions. The variation trend of the deviatoric stress-strain curve obtained under cyclic loading and unloading at the lower limit of variable stress after unloading is consistent with that of the curve obtained in Figure 4 under the same unloading amplitude. In the cyclic unloading stage at the first lower stress level, the primary pores and cracks in the coal samples gradually compacted. The three types of partial stress-strain curves were all concave in the first cyclic unloading stage, among which the more extensive the unloading amplitude was, the more pronounced the degree of concavity. Furthermore, the area of the first cyclic unloading hysteresis curve gradually decreased with the increase of the cycle number. After completing the first stage of cyclic loading and unloading, with the lower limit of stress level increase, the coal specimens under multistage circumferential pressure began to enter the elastic stage, in which the slope of the partial stress-strain cyclic loading and unloading curve became similar. The hysteresis curve area did not change much with the increase in the number of cycles, especially for the coal specimens that were not affected by the unloading effect. The second stage of the cyclic loading and unloading curve almost did not produce a hysteresis phenomenon. However, for the coal specimen C-6-3 with the unloading amplitude of 6 MPa, damage occurred after completing the first stage of cyclic unloading and failing to reach the upper limit stress set for the second stage of cyclic unloading.

The number of cyclic loading and unloading stages included in the σ_D-ε_1 curves of the coal specimens under the above unloading conditions was different. The number of cyclic loading and unloading stages included in the lower limit of variable stress for the coal specimens under the unloaded, unloaded amplitude of 3 MPa, and unloaded amplitude of 6 MPa conditions were 4, 3, and 1, respectively, which indicates that the damage of the coal specimens deepens with an increase in the unloading amplitude and become more easily damaged. The strains in the specimens increased with the increase of partial stress, and the area encompassed by the hysteresis curve increased significantly during the last level of cyclic unloading and unloading stages. In this case, the sample gradually transitioned to the plastic stage, and irreversible deformation continued to develop. The peak loads of the unloaded damaged coal specimens after the variable stress lower limit cycle unloading and unloading all slightly increased in the 9 MPa enclosing pressure environment compared with the conventional unloaded damaged coal specimens. After the variable stress lower limit cycle unloading and unloading, the peak stresses of the coal specimens with the unloading magnitude of 6 MPa, 3 MPa, and unloaded increased by 2.6%, 4.9%, and 6.2%, respectively, it indicates that the mechanical strength of the

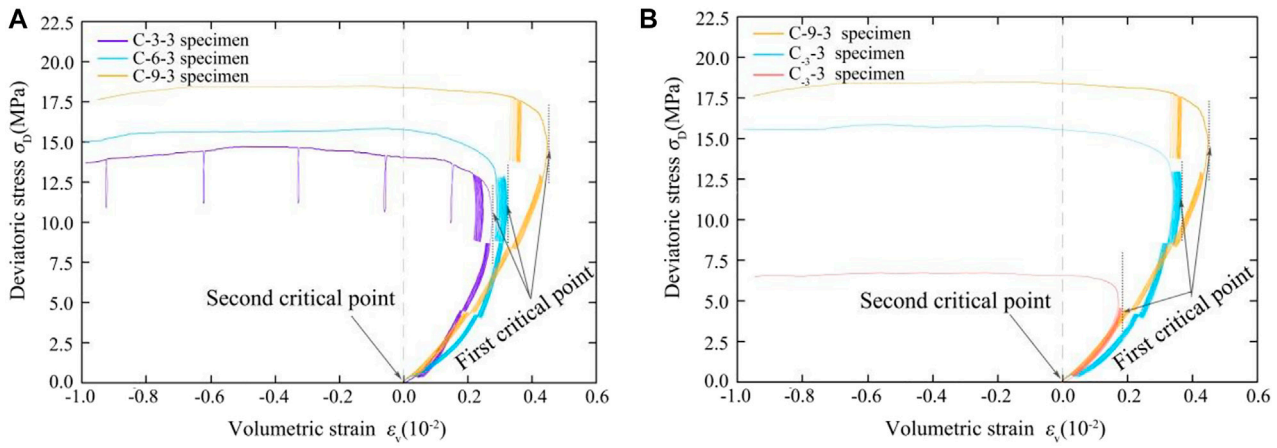

FIGURE 7
Deviatoric stress-volumetric strain (σ_D-ε_v) curves of coal specimens with cyclic loading and unloading at different stress lower limits **(A)** under different confining pressure; **(B)** under different unloading conditions.

coal specimens improved after the variable lower limit cycle unloading and unloading. The mechanical strength of the coal specimens improved to some extent after the variable lower limit cycle.

3.2 Volumetric strain ε_v characteristic

3.2.1 ε_v of coal specimens under different confining pressures

In the process of the above two types of tests, axial and radial extensometers were used to measure and record the normal strain ε_1 and radial strain ε_2 (ε_3) in the whole process of the test, where ε_2 is equivalent to ε_3. The volumetric strain ε_v during the coal specimen test was calculated by the following formula (Bruning et al., 2018):

$$\varepsilon_v = \varepsilon_1 - 2\varepsilon_2 \quad (1)$$

The direction of compression deformation is a positive value, and the direction of outward deformation is negative. When the calculated volumetric strain ε_v is positive, it indicates that the overall volume of the coal specimen is in the state of compression and reduction. When the calculated volumetric strain ε_v is negative, it indicates that the overall volume of the coal specimen is in a state of expansion.

Figure 7A depicts the evolution curves of volumetric strain and deviatoric stress of coal specimens under cyclic loading and unloading at the lower limit of variable stress under confining pressures of 3 MPa, 6 MPa, and 9 MPa, respectively. When coal specimens under different confining pressures were at a low cyclic stress level, the hysteresis curves were narrow and very close to each other. The slope of the curve at this stage was positive. It indicates that the current coal specimen was in a volumetric compression stage. The hysteresis curve gradually widened when the stress level gradually increased, and the width between curves increased during each loading and unloading cycle. This phenomenon was pronounced in the last loading and unloading cycle under each confining pressure condition. The slope of the test curve gradually changed from positive to negative, indicating that the volumetric strain of the coal specimen gradually changed from compression to expansion. The moment when the slope of the curve changed to zero was defined as the first critical point of volumetric strain. Before the critical point, the axial strain was dominant, and the coal specimen as a whole was continuously compressed until the slope of the curve was zero, reaching the minimum volumetric strain. Under the confining pressures of 3 MPa, 6 MPa, and 9 MPa, the volumetric strain at the first critical point was 0.25%, 0.31%, and 0.43%, respectively, and the corresponding deviatoric stress values were 10.5 MPa, 12.1 MPa, and 15.8 MPa, respectively. The volumetric compressive strain at the first critical point increased with the increase in confining pressure. After reaching the first critical point of volumetric strain, the axial stress continued to increase, and the volume of the coal specimen gradually increased from its minimum value. This change generally occurred at the last cyclic stress stage, indicating that damage accumulated inside the coal specimen and entered the plastic deformation stage. Under confining pressures of 3 MPa, 6 MPa, and 9 MPa, the volumetric strain of coal specimens at this stage increased by 0.32%, 0.24%, and 0.17%, respectively, indicating that the greater the confining pressure, the stronger the constraint on the radial deformation of coal specimens. When an axial load was further applied, the volumetric strain reverted to the initial hydrostatic pressure stage. Compared with the original specimen initially applied to confining pressure, the absolute value of volumetric strain at this time was zero, defined as the second critical point of volumetric strain. Volume strain of coal specimens under different confining pressure conditions above the critical point approximation commonly occurs when stress peak load, stress, more than the critical point for applying coal specimen instability occurs, more than the initial volume moment specimen volume and volume strain of coal specimen has entered into the phase of rapid growth. This is because the deviatoric stress under the action of coal specimen dilatancy damage occurred (Yang et al., 2021c).

3.2.2 ε_v of coal specimens under different unloading conditions

Figure 7B depicts the evolution curves of volumetric strain and deviatoric stress of the coal specimen under the conditions of no unloading, the unloading amplitude of 3 MPa, and the unloading amplitude of 6 MPa after cyclic loading and unloading at the lower

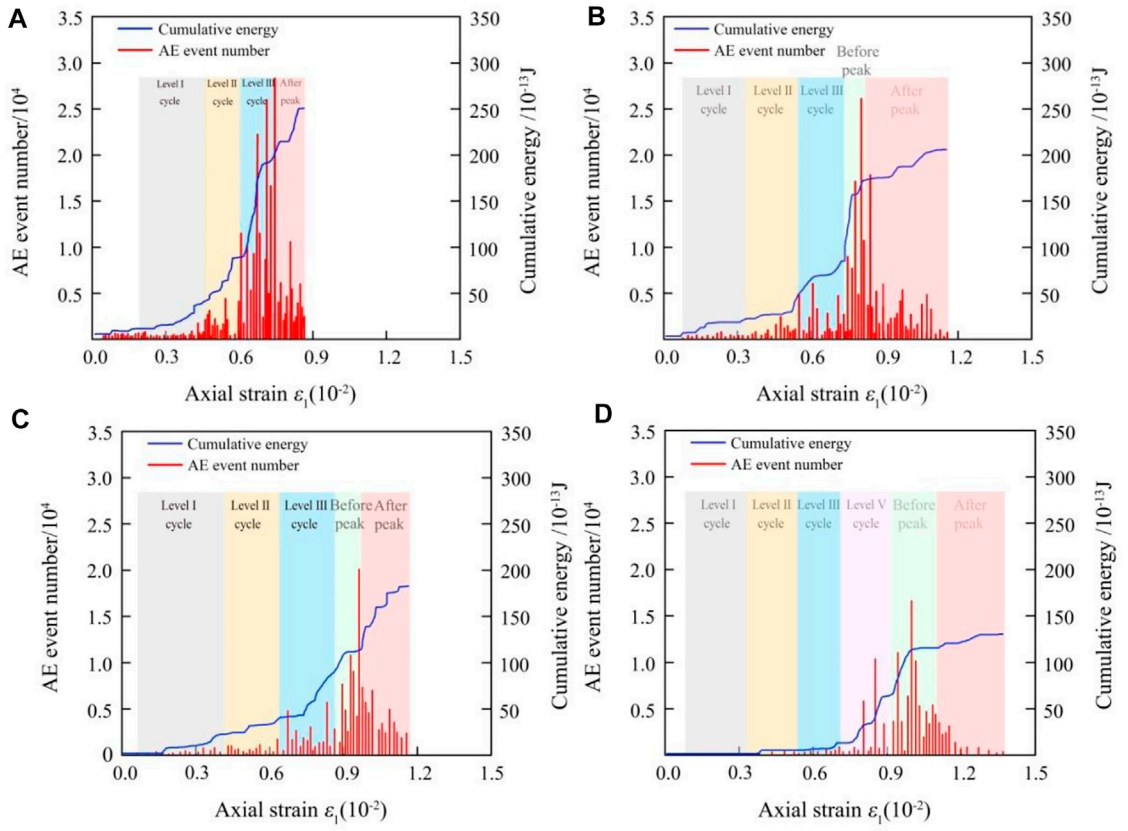

FIGURE 8
AE cumulative energy and AE event number of coal specimens with cyclic loading and unloading at different stress lower limits **(A)** under normal pressures, **(B)** under 3 MPa confining pressure, **(C)** under 6 MPa confining pressure, and **(D)** under 9 MPa confining pressure.

limit of variable stress. As shown in Figure 7B, the confining pressure of the coal specimens after the unloading with different amplitudes was raised to 9 MPa again. The hysteresis phenomenon was not evident at lower cyclic stress levels. ε_v was a positive value in this stage, indicating that the volume of the coal specimen was compressed within the cycle range. Concurrently, the slope of the summary curve of the process was positive, indicating that the current volume of the coal specimen was continuously compressed.

When the cyclic stress level increased, the hysteresis curves of the three types of specimens gradually widened during each cyclic loading and unloading process. This phenomenon was undeniable in the last stage of cyclic loading and unloading of each coal specimen. The slope of the test curve gradually changed from positive to negative, indicating that the volume of the coal specimen was continuously compressed to the minimum value and began to expand continuously. The moment when the slope of the curve becomes zero in this process is defined as the first critical point of volumetric strain. Before this critical point, the axial strain dominates, and the coal specimen as a whole appears to be continuously compacted until the minimum volumetric strain is reached when the slope of the curve is zero.

Under the conditions of no unloading, the unloading amplitude of 3 MPa, and the unloading amplitude of 6 MPa, the volumetric strain when reaching the first critical point was 0.43%, 0.31%, and 0.22%, respectively. The corresponding deviatoric stress values were 15.8 MPa and 12.11 MPa, and 10.23 MPa, respectively. Overall, with an increase in the unloading amplitude, the volume compressive strain value at the first critical point decreased continuously. When the first critical point of volumetric strain was reached, the axial stress continued to increase, and the volume of the coal specimen gradually increased from the minimum value. This change generally occurred in the last stage of cyclic stress on the coal specimen, indicating that the coal body deformation entered the plastic stage during this process. When the axial load was further applied, the volumetric strain returned to the initial stage as a whole. Compared with the coal specimen before the variable stress lower limit cyclic loading and unloading, the absolute value of the volumetric strain at this moment was zero, defined as the second critical point of the volumetric strain. The second critical point of the volumetric strain of coal specimens under different unloading conditions generally occurred when the stress reached the peak load. When the stress was continuously applied beyond this critical point, the coal specimen became unstable, the volume exceeded the initial volume, and the volumetric strain of the coal specimen entered a stage of rapid growth.

3.3 AE characteristic

3.3.1 AE characteristics of coal specimens under different confining pressures

As shown in Figure 1, five R3a acoustic emission sensors (preamplifiers) were used to monitor the evolution of acoustic emission events during the cyclic loading and unloading process of

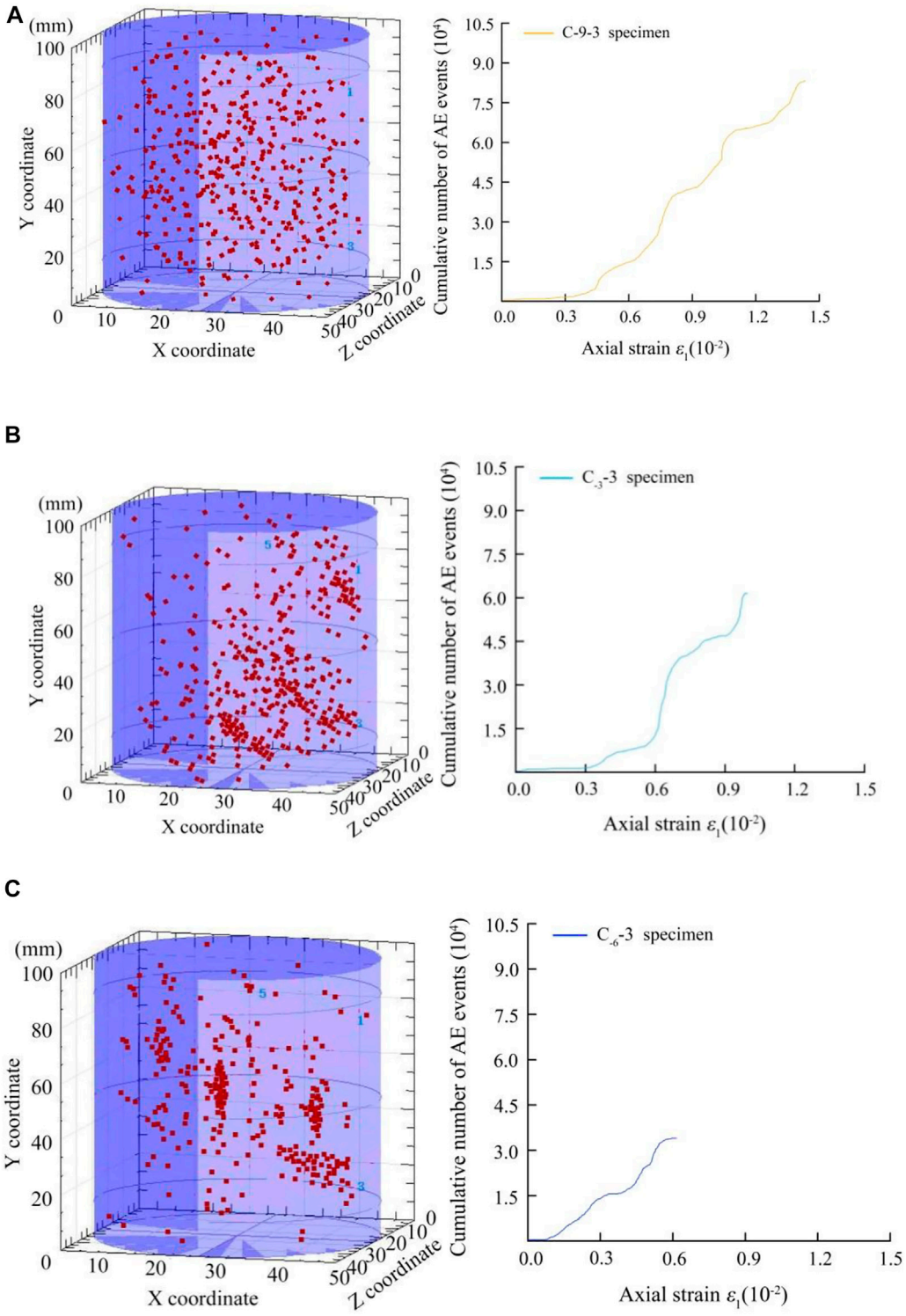

FIGURE 9
Acoustic emission characteristics of coal specimens under different unloading conditions.

the variable stress lower limit of the coal specimen under two types of test conditions.

Figure 8 depicts the cumulative energy change of acoustic emission of coal specimens loaded and unloaded under the conditions of normal pressure, a confining pressure of 3 MPa, confining pressure of 6 MPa and confining pressure of 9 MPa, and the number acoustic emission events in each stage of the test. As shown in Figure 8A, under the action of low cyclic stress at normal pressure, a small number of acoustic emission events occurred inside the coal specimen, indicating that a certain degree of damage occurred in the coal specimen during the initial compaction stage. With an increase in stress level, the acoustic emission events in the coal specimen gradually increased.

Acoustic emission events increased significantly during the last stage of cyclic loading and unloading. When approaching peak load, the increased rate of the acoustic emission events reached its peak value, and the macroscopical failure occurs in the post-peak residual strain stage of coal samples.

At the lower stress cyclic loading and unloading stage, as the confining pressure increased, the number of acoustic emission events gradually decreased. This shows that, under gradually increasing confining pressure, the internal structure of the coal specimen was gradually compressed, and the elastic deformation stage gradually expanded. As the cyclic stress level increased, the number of acoustic emission events gradually increased. When all the above three confining pressures entered the last stage of cyclic loading and unloading, the coal specimens suffered irreversible stress damage and fracturing. The number of acoustic emission events increased significantly. However, the higher the confining pressure, the smaller the growth rate of acoustic emission events. The total cumulative acoustic emission events of coal specimens under atmospheric pressure was 23.25×10^4. The cumulative total acoustic emission events of coal specimens under confining pressure conditions of 3 MPa, 6 MPa, and 9 MPa were 19.78×10^4, 12.32×10^4, and 8.16×10^4, respectively. Compared with the coal specimen without confining pressure, the cumulative events of acoustic emission under variable stress lower limit cyclic loading and unloading were reduced by 14.9%, 47.0%, and 64.9%, respectively (Figures 8B–D). This shows that a larger confining pressure environment restricts the formation of new tiny crack surfaces in the coal body due to the deviatoric stress. Overall, slight damage and fracturing events in the coal body are reduced.

As the confining pressure increased from normal pressure to 9 MPa, the cumulative energy of acoustic emission decreased from 256×10^{-13} J to 138×10^{-13} J, and the cumulative number of post-peak acoustic emission events decreased from 6.18×10^4 to 1.52×10^4. This shows that under the action of higher confining pressure, the coal body gradually changed from the brittle failure mode to the ductile failure mode.

3.3.2 AE characteristics of coal specimens under different unloading conditions

Figure 9 shows the lower limit cyclic loading and unloading path of variable stress, the cumulative number change of acoustic emission events of coal specimen, and the three-dimensional positioning cloud diagram of acoustic emission events when the peak load is 95% under the conditions of no unloading, unloading amplitude of 3 MPa and unloading amplitude of 6 MPa. When the coal specimen without unloading was nearing failure after the above test, the distribution of acoustic emission events in the coal specimen was scattered, and there was no significant internal damage fracture agglomeration area. When the coal specimen experienced unloading damage near the failure point, the acoustic emission events accumulated in several fixed areas. This phenomenon became more evident with the increasing unloading amplitude of the coal specimens. The reason is that the coal specimen without unloading under the confining pressure of 9 MPa can be considered a complete and continuous solid material. The damage and fracture inside the sample are randomly distributed when it is close to failure, resulting in a more dispersed position of internal acoustic emission events. However, for the coal samples with unloading damage, the number of micro defects contained in the coal samples increases, then uneven damage occurs under external loads. Some areas have a greater degree of damage, resulting in more significant damage from the severe damage, and ultimately, the acoustic emission events gather in some fixed areas inside the coal specimen. At the same time, with the increase in the unloading range of coal specimens, the number of cumulative acoustic emission events in the lower limit cyclic loading and unloading test process of variable stress under the triaxial environment of coal specimens decreases continuously.

Under the condition of no unloading, the cumulative total number of acoustic emission events of coal specimens was 8.16×10^4. Under the unloading amplitudes of 3 MPa and 6 MPa, the cumulative total number of acoustic emission events of coal specimens was 6.05×10^4 and 2.83×10^4, respectively. Compared with the unloaded coal sample, the cumulative acoustic emission events decreased by 25.9% and 65.3%, respectively. It shows that a more extensive unloading range causes more significant damage to the coal body and reduces the total energy required for the coal body to break.

Figure 10 shows the failure modes of coal specimens after cyclic loading and unloading at the lower limit of variable stress at 9 MPa confining pressure under the above different unloading amplitudes. With the increase in unloading amplitude, the final failure of coal specimens became increasingly broken, and the failure form gradually changed from ductile to brittle failure.

4 Discussion

4.1 Strain energy of coal

Figure 11 shows the typical axial stress-strain curves of coal specimens during each cyclic loading and unloading process of the above tests. The strain difference between the end of unloading and the beginning of loading in a cycle is called irreversible strain. The irreversible strain of the nth cyclic is ε^{U}_{n}-ε^{L}_{n}. It is due to a series of irreversible damage, such as the further expansion of microcracks in coal, plastic deformation of the coal skeleton, and friction between microcrack surfaces under various external physical forces (mostly stress fields). The macroscopic strain after unloading cannot be restored to the initial level of this cyclic loading. In addition, Figure 11 also gives the theoretical calculation examples of various strain energy in the cyclic loading and unloading of coal specimens. It is assumed that the above test process is a closed system and does not exchange heat with the outside world. Taking the nth cyclic loading and unloading as an example, the input energy U_{in}^{n} is the area covered by the stress-strain curve in the loading stage. The elastic strain energy U_{e}^{n} is the area value of the envelope under the unloading stage curve. The dissipated strain energy U_{d}^{n} is the difference between input and elastic strain energies. The specific calculation formula is as follows:

$$U_{in}^{n} = \int_{\varepsilon_n}^{\varepsilon_n^L} \sigma d\varepsilon \tag{2}$$

$$U_{e}^{n} = \int_{\varepsilon_n^U}^{\varepsilon_n} \sigma d\varepsilon \tag{3}$$

$$U_{d}^{n} = U_{in}^{n} - U_{e}^{n} \tag{4}$$

where ε^{L}_{n} is the strain value at the beginning of loading in the nth cycle. ε^{U}_{n} is the strain value after the nth unloading complete cycle. ε_n is the strain value at the peak time of the nth cyclic loading. ε_c is the strain

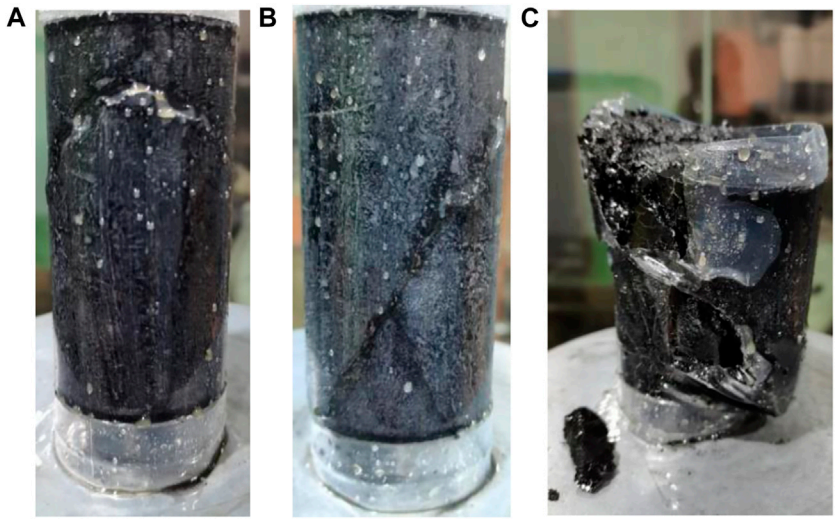

FIGURE 10
Failure modes of coal specimens **(A)** under not unloading, **(B)** under 3 MPa amplitude unloading condition, and **(C)** under 6 MPa amplitude unloading condition.

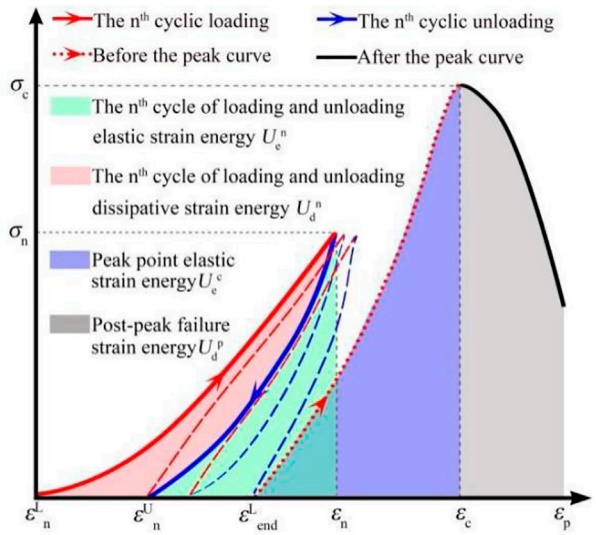

FIGURE 11
Schematic diagram of strain energy during cyclic loading and unloading of coal samples.

value when the final load reaches the peak load. ε_p is the strain value at the final failure time.

4.1.1 The energy storage law of coal specimens under different confining pressure

After the coal specimens under different confining pressure conditions are subjected to multistage variable stress lower limit cyclic loading and unloading, the calculation results of all types of strain energy in the last cycle of each stage of cyclic loading and unloading are shown in Table 3. According to the above results, with the increase of confining pressure, coal specimens' input energy and elastic strain energy at all levels of cyclic loading and unloading increase. The reason for this is that the overall mechanical strength of the coals is increased by the surrounding pressure. With the increase of the external load, the energy accumulated in the coal body before the destruction is continuously increased. It can be seen from the test results that for the same stage of cyclic loading and unloading, with the increase in confining pressure, the dissipated strain energy U_d^n of coal specimens gradually decreases. It shows that confining pressure can effectively restrain the increase of irreversible strain in a coal body.

Furthermore, the test results show that there is a linear relationship between the input energy U^n_{in} and the elastic strain energy U^n_e during the cyclic loading and unloading of the same coal sample under normal pressure, 3 MPa confining pressure, 6 MPa confining pressure, and 9 MPa confining pressure. The final fitting formula between the two is: $U^n_e=1.055U^n_{in}-0.416$. The goodness of fit is 0.996. This is consistent with the conclusion of (Gong et al., 2021).

4.1.2 The energy storage law of coal specimens under different unloading conditions

After different unloading effects, the coal specimens are subjected to multistage cyclic loading and unloading at the lower limit of variable stress. The calculation results of various strain energy in the last cyclic loading and unloading of each stage are listed in Table 4. According to the above calculation results, with the increase of unloading amplitude, in the confining pressure environment of 9 MPa, the input energy and elastic strain energy at all levels of cyclic loading and unloading decrease. Because the unloading effect causes damage to the coal body, the overall mechanical strength continues to decrease. It can be seen from the test results that, compared with the coal specimens without unloading, for the same level of cyclic loading and unloading stage, with the increase in unloading amplitude, the dissipated strain energy U_d^n of coal specimens gradually increases. Unloading can increase the irreversible strain in coal. In addition, there is a linear correlation between the input energy U^n_{in} and the elastic strain energy U^n_e under the conditions of no unloading, unloading amplitude 3 MPa, and unloading amplitude 6 MPa. The

TABLE 3 Cyclic loading and unloading test results of coal specimens under varying confining pressures.

Confining pressure	Specimen number	Level I cycle/ KJ·m^{-3}		Level II cycle/ KJ·m^{-3}		Level III cycle/ KJ·m^{-3}		Level V cycle/ KJ·m^{-3}		σ_c/MPa	U_e^c/kJ·m^{-3}	U_d^p/ kJ·m^{-3}
		U_{in}^n	U_e^n	U_{in}^n	U_e^n	U_{in}^n	U_e^n	U_{in}^n	U_e^n			
normal pressure	C-0-3	18.12	15.71	23.87	20.12	27.02	23.48	—	—	11.54	30.18	17.86
	C-0-4	17.82	15.14	21.89	18.42	25.72	22.10	—	—	10.06	27.74	9.54
3 MPa	C-3-3	25.12	22.14	29.30	26.76	33.75	31.42	—	—	16.21	38.69	21.74
	C-3-4	26.37	23.79	30.83	28.81	34.91	32.95	—	—	17.85	36.71	16.50
6 MPa	C-6-3	33.28	30.57	37.02	35.21	40.88	39.35	—	—	21.79	43.24	23.07
	C-6-4	34.82	32.83	38.10	36.67	42.22	40.95	—	—	23.97	45.38	21.93
9 MPa	C-9-3	41.52	39.47	45.28	43.51	48.67	47.32	51.29	49.48	27.23	55.23	31.45
	C-9-4	43.02	40.89	46.87	45.05	49.71	48.57	52.85	50.74	29.57	57.02	28.40

TABLE 4 Cyclic loading and unloading test results of coal specimens under varying amplitude unloading.

Unloading amplitude	Specimen number	Level I cycle/ KJ·m^{-3}		Level II cycle/ KJ·m^{-3}		Level III cycle/ KJ·m^{-3}		Level V cycle/ KJ·m^{-3}		σ_c/MPa	U_e^c/kJ·m^{-3}	U_d^p/ kJ·m^{-3}
		U_{in}^n	U_e^n	U_{in}^n	U_e^n	U_{in}^n	U_e^n	U_{in}^n	U_e^n			
Not unloading	C-9-3	41.52	39.47	45.28	43.51	48.67	47.32	51.29	49.48	27.23	55.23	31.45
	C-9-4	43.02	40.89	46.87	45.05	49.71	48.57	52.85	50.74	29.57	57.02	28.40
−3 MPa	C-3-3	35.17	33.21	38.53	36.96	42.74	41.65	—	—	24.05	43.87	23.42
	C-3-4	34.51	32.09	37.14	36.08	41.85	40.28	—	—	22.86	41.72	20.84
−6 MPa	C-6-3	23.42	20.11	—	—	—	—	—	—	14.96	30.51	19.75
	C-6-4	25.54	22.28	—	—	—	—	—	—	16.22	33.77	21.15

final fitting formula between the two is U^m_e=1.052U^m_{in}−4.056. The goodness of fit is 0.997. This is consistent with the conclusion of (Gong et al., 2021).

4.2 Bursting liability of coals

4.2.1 Effect of confining pressure and unloading on the coal bursting liability

In this study, the residual elastic energy index (C_{EF}) was used to analyze the rock burst tendency of coal specimens after cyclic loading and unloading of variable stress lower limits under different confining pressure conditions. According to the specific definition of residual elastic energy index (C_{EF}), when (C_{EF}) is less than 15 KJ m^{-3}, the coal sample has no rock burst tendency. The coal sample has a strong rock burst tendency when (C_{EF}) is more than 30 KJ m^{-3}. The coal sample has a weak rock burst tendency when (C_{EF}) is more than 15 KJ m^{-3} and less than 30 KJ m^{-3}. The residual elastic energy index (C_{EF}) is calculated as follows.

$$C_{EF} = U_e^c - U_d^p \quad (5)$$

In the formula, U_e^c is the peak load point elastic strain energy, that is, the elastic energy stored in the coal specimen before the peak load. The area under the peak front curve of coal specimens under different confining pressures can be brought into the linear relationship equation between input energy and elastic energy of coal samples established in the previous section to obtain the U_e^c under different confining pressure conditions. U_d^p is the post-peak damage strain energy, i.e., the area value of the envelope under the post-peak residual strain curve.

After calculation, the average residual elastic energy index value of the coal specimen under normal confining pressure conditions is 15.26 KJ m^{-3}, which indicates that this coal sample has a weak rock burst tendency under the action of the lower limit of variable stress with the room confining pressure. As shown in Figure 12A, under 3 MPa, 6 MPa, and 9 MPa confining pressures, the residual elastic energy index (C_{EF}) of coal specimen after cyclic loading and unloading under the lower limit of variable stress is 21.76%, 42.92%, and 71.69% higher than that under normal confining pressure. The above test results show that the confining pressure can enhance the rock burst tendency of the coal body. With increasing confining pressure, the strengthening effect on rock burst tendency propensity is constantly enhanced. In addition, the residual elastic energy index (C_{EF}) after multistage confining pressure and confining pressure σ_2 has a linear function relationship, with the formula C_{EF} = 1.214σ_2 + 14.97. With

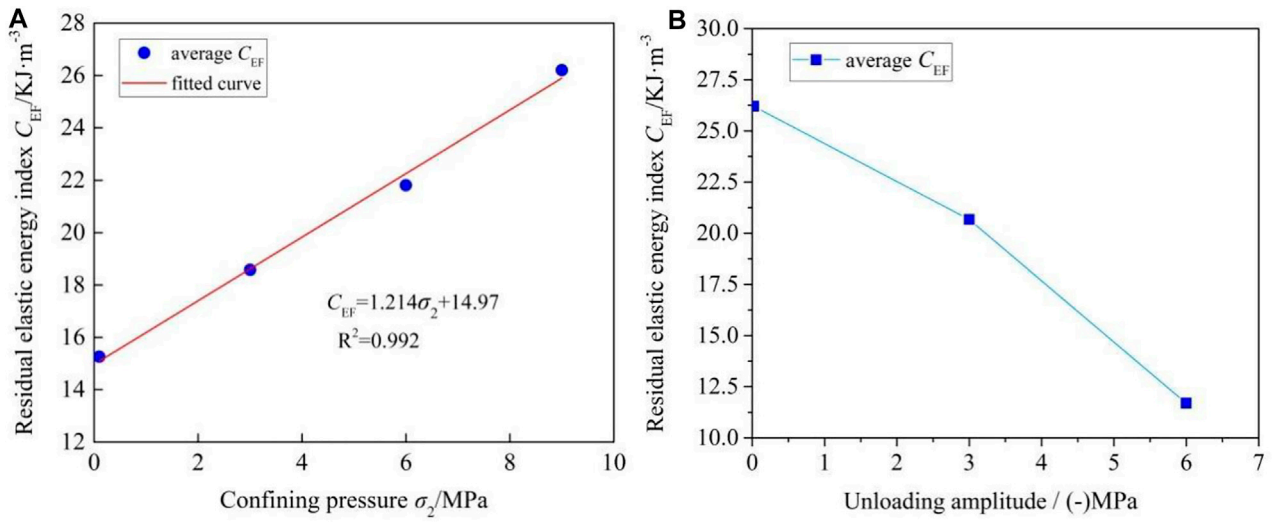

FIGURE 12
Residual elastic energy index of coal specimen **(A)** under confining pressure conditions and **(B)** under unloading conditions.

the increase of confining pressure, the rock burst strength of the coal body increases linearly.

As shown in Figure 12B, under the 9 MPa confining pressure, the (C_{EF}) of the coal specimen after unloading under the lower limit of the variable stress of 3 MPa and 6 MPa is 21.11% and 55.38% lower than that of the coal specimen without unloading. The test results show that the unloading effect weakens the coal body rock burst tendency. Furthermore, the weakening effect on the coal body rock burst tendency increases with the increase of unloading amplitude. The intensity and probability of coal rock bursts can be effectively reduced by releasing pressure coal in deep mines.

5 Conclusion

In this paper, lower-limit cyclic loading and unloading tests of variable stress were carried out on coal specimens with different unloading levels under multistage confining pressure. The purpose of this paper was to study the influence of confining pressure and unloading on the burst tendency of the coal body. The main conclusions are as follows:

1) The compressive strength of coal specimens under 3 MPa, 6 MPa, and 9 MPa confining pressure increased by 3.1%, 4.7%, and 6.2%, respectively, after cyclic loading and unloading under the lower limit of variable stress. At the same time, at the last stage of cyclic loading and unloading of the coal specimen under the above-confining pressure conditions, the coal specimen entered the plastic deformation process, in which the axial strain increased by .61%, .42%, and .28% respectively. The volumetric strain increased by .32%, .24%, and .17% respectively. This indicates that the greater the surrounding pressure on the coals, the stronger the constraint on the deformation of the coals. This improves the overall mechanical properties of the coal body.
2) Compared with the unloaded coal specimen under the confining pressure of 9 MPa, the compressive strength of the coal specimen decreased by 14.7% and 45.1%, respectively. The elastic modulus decreased from 2.42 GPa to 1.96 GPa and 1.24 GPa, respectively, after unloading the coal specimen with 3 MPa and 6 MPa, respectively. With the increase in unloading level, the peak load of the coal specimen decreased, the corresponding strain value decreased, and the post-peak deformation gradually decreased. The failure mode of the coal specimen gradually changed from ductile to brittle failure.
3) When the confining pressure of the coal specimen increased from the normal confining pressure to 9 MPa, the cumulative number of acoustic emission events during the cyclic loading and unloading of the lower limit of the variable stress of the coal specimen increased from 20.8×10^4 reduced to 8.6×10^4. The cumulative number of post-peak acoustic emissions of 7.5×10^4 was reduced to 3.2×10^4, and the accumulated energy was from 256×10^{-13} J to 158×10^{-13} J. This shows that the coal specimen becomes more compact with an increase in confining pressure, and the failure mode gradually transits from brittle failure to ductile failure. In addition, with the increase in the unloading level of coal specimens, the acoustic emission events in the lower limit cyclic loading and unloading test of variable stress gradually change from a dispersion state to several specific areas. When the unloading level was 3 MPa and 6 MPa, respectively, the total cumulative numbers of acoustic emission events of the coal specimen were 6.05×10^4 and 2.83×10^4. Compared with the coal specimen without unloading, the cumulative acoustic emission events decreased by 25.9% and 65.3%, respectively, indicating that the larger unloading level causes more significant damage to the coal body and reduces the total energy required for a coal body to fail.
4) With the increase in confining pressure, the irreversible strain of coal specimens at all cyclic loading and unloading levels gradually decreases. At the same time, the input energy U^n_{in} and elastic strain

energy U^n_e continuously increase. Under multistage confining pressure, there is a linear relationship between the elastic strain energy U^n_e and the input energy U^n_{in} during the cyclic loading and unloading of coal samples. In addition, with the increase in the unloading level, the irreversible strain of the coal specimen during the loading and unloading cycles at all levels gradually increases, and the input energy U^n_{in} and the elastic strain energy U^n_e continuously decrease. There is also a linear functional relationship between the elastic strain energy U^n_e and the input energy U^n_{in} of the coal samples during cyclic loading and unloading under different unloading level conditions.

5) Compared with the coal specimen under normal confining pressure, the residual elastic energy index (C_{EF}) of the coal specimen increased by 21.76%, 42.92%, and 71.69%, respectively, after cyclic loading and unloading under the lower limit of variable stress with the confining pressure of 3 MPa, 6 MPa, and 9 MPa, respectively. This shows that the confining pressure strengthens the rock burst tendency of the coal body. With an increase in confining pressure, the strengthening effect on the rock burst tendency of the coal body continuously increases. Furthermore, the residual elastic energy index (C_{EF}) has a linear functional relationship with the confining pressure. On the contrary, unloading has a weakening effect on the burst tendency of the coal body; and with the increase in unloading level, the weakening effect on the burst tendency of the coal body continues to increase.

Data availability statement

The original contributions presented in the study are included in the article/supplementary material, further inquiries can be directed to the corresponding author.

Author contributions

TD wrote the manuscript, JP and YX edited and revised it, and RS did the experiments.

Conflict of interest

TD, JP, YX, and RS are employed by the company Tiandi Science and Technology Co., Ltd.

Publisher's note

References

Bruning, T., Karakus, M., Nguyen, G. D., and Goodchild, D. (2018). Experimental study on the damage evolution of brittle rock under triaxial confinement with full circumferential strain control. *Rock Mech. Rock Eng.* 51 (11), 3321–3341. doi:10.1007/s00603-018-1537-7

Cai, W., Dou, L., Si, G., Cao, A., He, J., and Liu, S. (2016). A principal component analysis/fuzzy comprehensive evaluation model for coal burst liability assessment. *Int. J. Rock Mech. Min. Sci.* 81, 62–69. doi:10.1016/j.ijrmms.2015.09.028

Chen, Y., Liang, W., Lian, H., Yang, J., and Nguyen, V. P. (2017). Experimental study on the effect of fracture geometric characteristics on the permeability in deformable rough-walled fractures. *Int. J. Rock Mech. Min. Sci.* 98, 121–140. doi:10.1016/j.ijrmms.2017.07.003

Chen, Y., Lian, H., Liang, W., Yang, J., Nguyen, V. P., and Bordas, S. P. (2019). The influence of fracture geometry variation on non-Darcy flow in fractures under confining stresses. *Int. J. Rock Mech. Min. Sci.* 113, 59–71. doi:10.1016/j.ijrmms.2018.11.017

Ding, Z. W., Jia, J. D., Tang, Q. B., and Li, X. F. (2022). Mechanical properties and energy damage evolution characteristics of coal under cyclic loading and unloading. *Rock Mech. Rock Eng.* 55, 4765–4781. doi:10.1007/s00603-022-02884-x

Gong, F., Yan, J., Li, X., and Luo, S. (2019). A peak-strength strain energy storage index for rock burst proneness of rock materials. *Int. J. Rock Mech. Min. Sci.* 117, 76–89. doi:10.1016/j.ijrmms.2019.03.020

Gong, F. Q., Wang, Y. L., and Luo, S. (2020). Rockburst proneness criteria for rock materials: Review and new insights. *J. Central South Univ.* 27 (10), 2793–2821. doi:10.1007/s11771-020-4511-y

Gong, F., Wang, Y., Wang, Z., Pan, J., and Luo, S. (2021). A new criterion of coal burst proneness based on the residual elastic energy index. *Int. J. Min. Sci. Technol.* 31 (4), 553–563. doi:10.1016/j.ijmst.2021.04.001

Gong, F., Luo, S., Jiang, Q., and Xu, L. (2022). Theoretical verification of the rationality of strain energy storage index as rockburst criterion based on linear energy storage law. *J. Rock Mech. Geotech. Eng.* 14, 1737–1746. doi:10.1016/j.jrmge.2021.12.015

Guo, W. Y., Tan, Y. L., Yang, Z. L., Zhao, T. B., and Hu, S. C. (2018). Effect of saturation time on the coal burst liability indexes and its application for rock burst mitigation. *Geotech. Geol. Eng.* 36 (1), 589–597. doi:10.1007/s10706-017-0300-2

Kidybinski, A. (1981). Bursting liability indices of coal. *Int. J. Rock Mech. Min. Sci.* 18 (6), 295–304. doi:10.1016/0148-9062(81)91194-3

Kong, X., Wang, E., Li, S., Lin, H., Zhang, Z., and Ju, Y. (2020). Dynamic mechanical characteristics and fracture mechanism of gas-bearing coal based on SHPB experiments. *Theor. Appl. Fract. Mech.* 105, 102395. doi:10.1016/j.tafmec.2019.102395

Li, Y., Yang, S. Q., Liu, Z. L., Sun, B. W., Yang, J., and Xu, J. (2022a). Study on mechanical properties and deformation of coal specimens under different confining pressure and strain rate. *Theor. Appl. Fract. Mech.* 118, 103287. doi:10.1016/j.tafmec.2022.103287

Li, Y., Zhao, B., Yang, J., Sun, J., Huang, W., Li, Z., et al. (2022b). Experimental study on the influence of confining pressure and bedding angles on mechanical properties in coal. *Minerals* 12 (3), 345. doi:10.3390/min12030345

Liu, Q., Cheng, Y., Jin, K., Tu, Q., Zhao, W., and Zhang, R. (2017). Effect of confining pressure unloading on strength reduction of soft coal in borehole stability analysis. *Environ. Earth Sci.* 76 (4), 173–211. doi:10.1007/s12665-017-6509-9

Liu, X., Wang, X., Wang, E., Kong, X., Zhang, C., Liu, S., et al. (2017). Effects of gas pressure on bursting liability of coal under uniaxial conditions. *J. Nat. Gas Sci. Eng.* 39, 90–100. doi:10.1016/j.jngse.2017.01.033

Ouyang, Z., Qi, Q., Zhao, S., Wu, B., and Zhang, N. (2015). The mechanism and application of deep-hole precracking blasting on rockburst prevention. *Shock Vib.* 2015, 1–7. doi:10.1155/2015/625691

Wang, J., and Huang, Z. (2017). The recent technological development of intelligent mining in China. *Engineering* 3 (4), 439–444. doi:10.1016/j.eng.2017.04.003

Wang, D., Zhang, P., Wei, J., and Yu, C. (2020). The seepage properties and permeability enhancement mechanism in coal under temperature shocks during unloading confining pressures. *J. Nat. Gas Sci. Eng.* 77, 103242. doi:10.1016/j.jngse.2020.103242

Wang, D., Chen, F., Mao, J., Liu, N., and Rong, F. (2022). Are the official national data credible? Empirical evidence from statistics quality evaluation of China's coal and its downstream industries. *Energy Econ.* 2022, 106310. doi:10.1016/j.eneco.2022.106310

Wang, Q., Qin, Q., Jiang, B., Jiang, Z., He, M., Li, S., et al. (2020). Geomechanics model test research on automatically formed roadway by roof cutting and pressure releasing. *Int. J. Rock Mech. Min. Sci.* 135, 104506. doi:10.1016/j.ijrmms.2020.104506

Xie, H., Zhao, X., Liu, J., Zhang, R., and Xue, D. (2012). Influence of different mining layouts on the mechanical properties of coal. *Int. J. Min. Sci. Technol.* 22 (6), 749–755. doi:10.1016/j.ijmst.2012.12.010

Xie, H., Li, C., He, Z., Li, C., Lu, Y., Zhang, R., et al. (2021). Experimental study on rock mechanical behavior retaining the *in situ* geological conditions at different depths. *Int. J. Rock Mech. Min. Sci.* 138, 104548. doi:10.1016/j.ijrmms.2020.104548

Yang, J., Liang, W., Lian, H., Chen, Y., and Li, L. (2018a). "Influence of the different fluids on the hydraulic fracturing mechanism of sandy mudstone," in ISRM International Symposium-10th Asian Rock Mechanics Symposium, 2018, October (OnePetro).

Yang, J., Lian, H., Liang, W., Nguyen, V. P., and Chen, Y. (2018b). Experimental investigation of the effects of supercritical carbon dioxide on fracture toughness of bituminous coals. *Int. J. Rock Mech. Min. Sci.* 107, 233–242. doi:10.1016/j.ijrmms.2018.04.033

Yang, X., Ren, T., Tan, L., Remennikov, A., and He, X. (2018). Developing coal burst propensity index method for Australian coal mines. *Int. J. Min. Sci. Technol.* 28 (5), 783–790. doi:10.1016/j.ijmst.2018.08.008

Yang, J., Li, L., and Lian, H. (2019a). Experimental evaluation of the influences of water on the fracture toughness of mudstones with bedding. *Adv. Mater. Sci. Eng.* 2019, 1–16. doi:10.1155/2019/5693654

Yang, J., Lian, H., Liang, W., Nguyen, V. P., and Bordas, S. P. (2019b). Model I cohesive zone models of different rank coals. *Int. J. Rock Mech. Min. Sci.* 115, 145–156. doi:10.1016/j.ijrmms.2019.01.001

Yang, J., Lian, H., and Li, L. (2020a). Fracturing in coals with different fluids: An experimental comparison between water, liquid CO2, and supercritical CO2. *Sci. Rep.* 10 (1), 18681–18715. doi:10.1038/s41598-020-75787-y

Yang, J., Li, L., and Lian, H. (2020b). Experimental investigation of the effects of water content on the anisotropy of mode I fracture toughness of bedded mudstones. *Plos one* 15 (8), e0237909. doi:10.1371/journal.pone.0237909

Yang, J., Lian, H., and Li, L. (2021a). Investigating the effect of confining pressure on fracture toughness of CO2-saturated coals. *Eng. Fract. Mech.* 242, 107496. doi:10.1016/j.engfracmech.2020.107496

Yang, J., Ren, Y., Zhang, D., Liu, Y., and Ma, Z. (2021b). Numerical simulation of fracturing in coals using water and supercritical carbon dioxide with potential-based cohesive zone models. *Geofluids* 2021, 1–14. doi:10.1155/2021/7645382

Yang, J., Lian, H., and Nguyen, V. P. (2021c). Study of mixed mode I/II cohesive zone models of different rank coals. *Eng. Fract. Mech.* 246, 107611. doi:10.1016/j.engfracmech.2021.107611

Yin, G., Li, W., Jiang, C., Li, M., Li, X., Liu, H., et al. (2013). Mechanical property and permeability of raw coal containing methane under unloading confining pressure. *Int. J. Min. Sci. Technol.* 23 (6), 789–793. doi:10.1016/j.ijmst.2013.10.002

Yin, G., Jiang, C., Wang, J. G., and Xu, J. (2015). Geomechanical and flow properties of coal from loading axial stress and unloading confining pressure tests. *Int. J. Rock Mech. Min. Sci.* 76, 155–161. doi:10.1016/j.ijrmms.2015.03.019

Zhang, Q., Fan, X., Liang, Y., Li, M., Li, G., Ma, T., et al. (2017). Mechanical behavior and permeability evolution of reconstituted coal samples under various unloading confining pressures—Implications for wellbore stability analysis. *Energies* 10 (3), 292. doi:10.3390/en10030292

Zhang, X., He, M., Yang, J., Wang, E., Zhang, J., and Sun, Y. (2020). An innovative non-pillar coal-mining technology with automatically formed entry: A case study. *Engineering* 6 (11), 1315–1329. doi:10.1016/j.eng.2020.01.014

Zhou, H. W., Wang, L. J., Rong, T. L., Zhang, L., Ren, W. G., and Su, T. (2019). Creep-based permeability evolution in deep coal under unloading confining pressure. *J. Nat. Gas Sci. Eng.* 65, 185–196. doi:10.1016/j.jngse.2019.03.010

Zhou, H. W., Liu, Z. L., Zhong, J. C., Chen, B. C., Zhao, J. W., and Xue, D. J. (2022). NMRI online observation of coal fracture and pore structure evolution under confining pressure and axial compressive loads: A novel approach. *Energy* 261, 125297. doi:10.1016/j.energy.2022.125297

Zhou, J., Zhao, Y., Paneiro, G., Liu, W., Wang, X., Wang, H., et al. (2022). Loading rate and bedding plane coupled effect study on coal failure under uniaxial compression: Acoustic emissions and energy dissipation analysis. *Geofluids* 2022, 1–16. doi:10.1155/2022/9028178